Robust Performance Analysis Applied to Gust Loads Computation

(Received: July 8, 2013. Revised: Aug 21, 2013. Accepted: Dec. 12, 2013)

Andreas Knoblach[1]

Abstract
This paper demonstrates how the robust performance analysis framework can be used to determine worst case loads of flexible aircraft due to "1-cosine" gusts. This framework is a part of control theory and is used to characterize a system by input-output norms: e. g. the induced $\mathcal{L}_2$-$\mathcal{L}_\infty$ norm represents the worst case energy-to-peak gain. Two very efficient ways to compute this norm are presented. Based on the physical interpretation of this norm, an aircraft model is weighted such that the induced $\mathcal{L}_2$-$\mathcal{L}_\infty$ norm of the weighted system represents a close but guaranteed upper bound for "1-cosine" gusts and similar excitations. The analysis results are compared to simulations. Since the energy-to-peak gain can be computed in a very efficient way for linear time invariant (LTI) models, the norm is used to quickly obtain an upper bound for loads and to identify critical flight conditions. In a second example, the analysis is additionally performed on an uncertain model.

Nomenclature

$\boldsymbol{d}(t)$	Input vector
$\boldsymbol{e}(t)$	Output vector
$\boldsymbol{G}(\boldsymbol{\rho})$	Linear parameter-varying (LPV) system
$G(\boldsymbol{\rho})_{d\to e}$	LPV system: path from d to e
h	Flight level
Ma	Mach number
$\mathcal{P}$	Parameter space
P_{WRB}	Wing root bending (WRB) moment
$\boldsymbol{Q}$	Controllability Gramian matrix
$\boldsymbol{\rho}(t)$	Parameter vector
$\mathbb{R}/\mathbb{R}_+$	Set of real / nonnegative real numbers
$\ddot{u}_z$	Vertical acceleration
v_{gust}	Vertical wind
W	Weighting filter
$\boldsymbol{X}(\boldsymbol{\rho})$	Parameter dependent Lyapunov matrix
$\|\boldsymbol{x}\|_{\mathcal{L}_2}$	$\mathcal{L}_2$ signal norm of $\boldsymbol{x}(t)$ (energy norm)
$\|\boldsymbol{x}\|_{\mathcal{L}_\infty}$	$\mathcal{L}_\infty$ signal norm of $\boldsymbol{x}(t)$ (peak norm)
$\|\boldsymbol{G}\|_{\mathcal{L}_2\to\mathcal{L}_\infty}$	Induced $\mathcal{L}_2$-$\mathcal{L}_\infty$ norm of $\boldsymbol{G}$ (worst case energy-to-peak gain)
$\overline{(\cdot)}$	Normalized value of $(\cdot)$

1 Introduction

In order to certify a new aircraft, it must be proved that it can withstand loads caused by turbulence and gusts, see [6]. According to the CS-25 of the European Aviation Safety Agency (EASA) [1], two types of excitation have to be considered: discrete "1-cosine" gusts and continuous turbulence. In the first case, an aircraft model is excited with a single "1-cosine" gust profile and the model outputs, e. g. the wing root bending (WRB) moment or the vertical accelerations, are

[1] German Aerospace Center
Institute of System Dynamics and Control
82234 Weßling, GERMANY
andreas.knoblach@dlr.de

doi:10.3293/asdj.2013.21

computed. Next, the trim loads are superimposed and the procedure is repeated for several gust lengths. Moreover, the complete process has to be performed for lots of flight points such that the entire flight envelope (defined by velocity, altitude, loading etc.) is covered. Finally, the maximum and minimum peak of every output for all these simulations defines the limit loads due to discrete gusts. The other type of excitation – namely continuous turbulence – considers the stochastic nature of turbulence. Here, the von Karman wind turbulence model is used to excite the aircraft and the results are evaluated by stochastic means. The limit loads are derived from the root mean square (RMS) value of the model response. A detailed description of the discrete gusts and continuous turbulence scenarios can be found in [6].

Since these millions of simulations are very time consuming, there is a need for fast and reliable algorithms to identify worst case flight points and to compute maximum loads. Consequently, this problem is intensively studied in literature: in [20] the so called matched filter theory is used to compute worst case gusts. By exciting an aircraft with these gusts worst case loads can by identified. In [4], the RMS value of the aircraft model output due to white noise excitation is computed by solving a Lyapunov equation. The usage of surrogate modeling and optimization techniques is considered in [8] for identifying critical flight conditions and for predicting worst case gust loads.

Indeed, the approach from [4] is equivalent to computing the $\mathcal{H}_2$ norm for linear time invariant (LTI) systems and the considered interpretation is well known in control theory. However, there are further interesting system norms. In terms of loads computation, the induced $\mathcal{L}_2$-$\mathcal{L}_\infty$ norm is promising, because this norm specifies the worst case energy-to-peak gain, i. e. an upper bound for the output peak for all excitations with a maximum energy of one. By introducing a weighting filter, which is able to shape a "1-cosine" gust of arbitrary length with a maximum energy of one, an upper bound for gust loads can be directly computed. Moreover, the robust performance analysis framework allows the computation of these upper bounds also for uncertain and for linear parameter-varying (LPV) systems, see e. g. [3] and [5]. Consequently, this control theory method allows the computation of upper bounds for gust loads for a parameter dependent model by only one analysis. At this point, it is mentioned that this paper does not present the first application of robust control theory methods for an aeroelastic problem; in [11] and [2] the μ-analysis framework is used for flutter analysis.

The aim of this paper is to show how the worst case energy-to-peak gain can be used in the process of loads computation. The paper is structured as follows: an overview about important preliminaries is presented in Section 2. In Section 3, the induced $\mathcal{L}_2$-$\mathcal{L}_\infty$ norm is formally defined and it is explained how it can be computed. Next, in Section 4, LTI performance analyses are performed and compared to simulation results. It is shown how the energy-to-peak gain can be used to compute a close but guaranteed bound for the model output caused by a "1-cosine" gust excitation. In Section 5, the robust performance analysis is performed on an uncertain model. Finally, a summary and an outlook to further applications of the robust performance analysis for loads computation is presented in Section 6.

2 Preliminaries

In this section, LPV systems are briefly introduced and two important signal norms are defined.

2.1 Linear Parameter Varying Systems

In order to introduce the class of LPV systems, differentiable parameter vector trajectories are defined first. The time dependent parameter vector is defined as a function $\boldsymbol{\rho}\colon \mathbb{R}_+ \to \mathcal{P}$, where $\mathbb{R}_+$ is the set of all nonnegative real numbers,

the parameter space $\mathcal{P}$ is a compact subset of $\mathbb{R}^{n_\rho}$ and n_ρ is the number of parameters.

Definition 1 (LPV system [19])**:** The linear parameter-varying (LPV) system

$$\boldsymbol{G}(\boldsymbol{\rho}): \begin{cases} \dot{\boldsymbol{x}} = \boldsymbol{A}(\boldsymbol{\rho}(t))\boldsymbol{x} + \boldsymbol{B}(\boldsymbol{\rho}(t))\boldsymbol{d} \\ \boldsymbol{e} = \boldsymbol{C}(\boldsymbol{\rho}(t))\boldsymbol{x} + \boldsymbol{D}(\boldsymbol{\rho}(t))\boldsymbol{d} \end{cases} \tag{1}$$

maps an input vector $\boldsymbol{d} \in \mathbb{R}^{n_d}$ to an output vector $\boldsymbol{e} \in \mathbb{R}^{n_e}$, where the continuous matrix functions $\boldsymbol{A}\colon \mathcal{P} \to \mathbb{R}^{n_x \times n_x}$, $\boldsymbol{B}\colon \mathcal{P} \to \mathbb{R}^{n_x \times n_d}$, $\boldsymbol{C}\colon \mathcal{P} \to \mathbb{R}^{n_e \times n_x}$, $\boldsymbol{D}\colon \mathcal{P} \to \mathbb{R}^{n_e \times n_d}$ and a state vector $\boldsymbol{x} \in \mathbb{R}^{n_x}$ are used. The notation $G(\boldsymbol{\rho})_{d\to e}$ system is used to refer to the specific path from d to e.

LPV systems are hence very similar to the well-known LTI systems, with the difference that the system matrices depend on parameters. Figuratively speaking, these parameters can be considered as additional inputs, which alter the plant dynamics. Typical examples for parameters are the flight level or the Mach number.

Since the here considered parameters change very slowly, they are treated as time invariant, i. e. $\frac{\mathrm{d}\boldsymbol{\rho}(t)}{\mathrm{d}t} = 0$. However, for the sake of readability, the explicit time dependence of $\boldsymbol{\rho}$ is dropped below.

2.2 Signal Norms

An n-dimensional signal is a function of the time, i. e. $\boldsymbol{x}\colon \mathbb{R}_+ \to \mathbb{R}^n$. Two important signal norms are presented below.

Definition 2 ($\mathcal{L}_2$ signal norm [17])**:** The $\mathcal{L}_2$ norm of $\boldsymbol{x}(t)$ is defined as

$$\|\boldsymbol{x}\|_{\mathcal{L}_2} = \sqrt{\int_0^\infty \boldsymbol{x}(t)^{\mathrm{T}}\boldsymbol{x}(t)\mathrm{d}t}. \tag{2}$$

The $\mathcal{L}_2$ norm can be interpreted as the energy of a signal, so that it is also referred to as energy norm.

Definition 3 ($\mathcal{L}_\infty$ signal norm [17])**:** The $\mathcal{L}_\infty$ norm of $\boldsymbol{x}(t)$ is defined as

$$\|\boldsymbol{x}\|_{\mathcal{L}_\infty} = \sup_{t\geq 0} \sqrt{\boldsymbol{x}(t)^{\mathrm{T}}\boldsymbol{x}(t)}. \tag{3}$$

For scalar valued signals $x(t)$, the $\mathcal{L}_\infty$ norm corresponds to $\sup|x(t)|$. Hence, the $\mathcal{L}_\infty$ norm is also referred to as peak norm of a signal.[1]

3 Worst Case Energy-to-Peak Gain

Although the induced $\mathcal{L}_2$-$\mathcal{L}_2$ norm (or for LTI system also $\mathcal{H}_\infty$ norm) is commonly used in the robust performance analysis framework, the induced $\mathcal{L}_2$-$\mathcal{L}_\infty$ is more suited for loads computation since it allows the computation of an upper bound for the output peaks. It is formally defined below and two possibilities to compute it are presented.

3.1 Definition and Interpretation

Definition 4 ($\mathcal{L}_2$-$\mathcal{L}_\infty$ norm for LPV systems [5] and [16])**:** The induced $\mathcal{L}_2$-$\mathcal{L}_\infty$ norm for LPV systems $\|\boldsymbol{G}(\boldsymbol{\rho})\|_{\mathcal{L}_2\to\mathcal{L}_\infty}$ is defined by

$$\|\boldsymbol{G}(\boldsymbol{\rho})\|_{\mathcal{L}_2\to\mathcal{L}_\infty} = \sup_{\substack{\boldsymbol{d}\neq\boldsymbol{0},\boldsymbol{d}\in\mathcal{L}_2 \\ \boldsymbol{\rho}\in\mathcal{P}}} \frac{\|\boldsymbol{e}\|_{\mathcal{L}_\infty}}{\|\boldsymbol{d}\|_{\mathcal{L}_2}}. \tag{4}$$

[1] Note that the $\mathcal{L}_\infty$ signal norm is not uniquely defined in the literature. Throughout this paper, only Definition 3 is used.

It is easy to see that the induced $\mathcal{L}_2$-$\mathcal{L}_\infty$ norm corresponds to the worst case energy-to-peak gain. Hence, this norm allows to determine the maximum possible amplitude of the output if the input energy is less than or equal zero. The latter condition can be achieved by a suitable scaling of the system.

Note that a necessary condition for the $\mathcal{L}_2$-$\mathcal{L}_\infty$ norm being finite is that the feed-through matrix $\boldsymbol{D}(\boldsymbol{\rho}) = \mathbf{0}$. However, by adding a low-pass filter to the system the latter condition can always be fulfilled. Since the excitation signal is usually of a limited frequency range, the low-pass filter will not deteriorate the results if the cutoff frequency is chosen high enough. Moreover, the filter can be used to weight a relevant frequency range. Note that for LTI systems, the induced $\mathcal{L}_2$-$\mathcal{L}_\infty$ norm corresponds to the so called generalized $\mathcal{H}_2$ norm [16].

3.2 Computation via a Lyapunov Equation

The induced $\mathcal{L}_2$-$\mathcal{L}_\infty$ norm for an LTI system can be computed by solving the Lyapunov equation

$$\boldsymbol{A}\boldsymbol{Q} + \boldsymbol{Q}\boldsymbol{A}^{\mathrm{T}} + \boldsymbol{B}^{\mathrm{T}}\boldsymbol{B} = 0, \tag{5}$$

where $\boldsymbol{Q}$ is the so called controllability Gramian matrix. The Gramian matrix can be easily computed by Matlab using the command `gram`, see [13]. From $\boldsymbol{Q}$, the LTI $\mathcal{L}_2$-$\mathcal{L}_\infty$ can be computed as

$$\|\boldsymbol{G}(\boldsymbol{\rho})\|_{\mathcal{L}_2\to\mathcal{L}_\infty} = \max\left(\operatorname{eig}\left(\boldsymbol{C}\boldsymbol{Q}\boldsymbol{C}^{\mathrm{T}}\right)\right). \tag{6}$$

The advantage of computing the induced $\mathcal{L}_2$-$\mathcal{L}_\infty$ norm by a Lyapunov equation is that this approach is extreme fast and numerically robust. However, this approach is restricted to LTI systems. See [16] for details and proofs.

3.3 Computation via LMIs

As already mentioned, the computation of the induced $\mathcal{L}_2$-$\mathcal{L}_\infty$ norm by Lyapunov equations is not possible for LPV systems. However, it is possible to determine an upper bound for it by solving a semidefinite program (SDP). This approach is based on a linear matrix inequality (LMI) constraint for the induced $\mathcal{L}_2$-$\mathcal{L}_\infty$ norm: the LPV system $\boldsymbol{G}(\boldsymbol{\rho})$ is exponentially stable and its induced $\mathcal{L}_2$-$\mathcal{L}_\infty$ norm from $\boldsymbol{d}$ to $\boldsymbol{e}$ is smaller than a performance index γ if there exists a symmetric Lyapunov matrix $\boldsymbol{X}\colon \mathcal{P} \to \mathbb{S}^{n_x}$ s. t. $\forall \boldsymbol{\rho} \in \mathcal{P}$

$$\boldsymbol{X}(\boldsymbol{\rho}) > 0, \tag{7a}$$

$$\begin{bmatrix} \boldsymbol{A}(\boldsymbol{\rho})^{\mathrm{T}}\boldsymbol{X}(\boldsymbol{\rho}) + \boldsymbol{X}(\boldsymbol{\rho})\boldsymbol{A}(\boldsymbol{\rho}) & \boldsymbol{X}(\boldsymbol{\rho})\boldsymbol{B}(\boldsymbol{\rho}) \\ \boldsymbol{B}(\boldsymbol{\rho})^{\mathrm{T}}\boldsymbol{X}(\boldsymbol{\rho}) & -\gamma\mathbf{I} \end{bmatrix} < 0, \tag{7b}$$

$$\begin{bmatrix} \boldsymbol{X}(\boldsymbol{\rho}) & \boldsymbol{C}(\boldsymbol{\rho})^{\mathrm{T}} \\ \boldsymbol{C}(\boldsymbol{\rho}) & \gamma\mathbf{I} \end{bmatrix} > 0. \tag{7c}$$

In (7), the term $\boldsymbol{X} > 0$ means that $\boldsymbol{X}$ is positive definite.[2] An upper bound for $\|\boldsymbol{G}(\boldsymbol{\rho})\|_{\mathcal{L}_2\to\mathcal{L}_\infty}$ can be thus determined by solving the SDP

$$\min_{\gamma, \boldsymbol{X}(\boldsymbol{\rho})} \gamma \quad \text{s. t. (7) is fulfilled } \forall \boldsymbol{\rho} \in \mathcal{P}. \tag{8}$$

The decision variables of this convex optimization problem are the entries of the Lyapunov matrix $\boldsymbol{X}(\boldsymbol{\rho})$ and the performance index γ. SDPs can be solved in a numerically efficient way by Interior-Point methods. LMIs can be easily coded using the LMI parser YALMIP [12]. Throughout this paper, the SDP solver SDPT3 [18] is used to solve the resulting optimization problems. Further details

[2] A symmetric matrix $\boldsymbol{X}$ is positive definite if all eigenvalues of $\boldsymbol{X}$ are positive. Analogously, $\boldsymbol{X} < 0$ means negative definiteness of $\boldsymbol{X}$. Note that $\boldsymbol{X} > 0 \Leftrightarrow -\boldsymbol{X} < 0$.

as well as a proof for the LMI constraint of the induced $\mathcal{L}_2$-$\mathcal{L}_\infty$ norm can be found in e. g. [5] and [16].

There are still two problems in the SDP (8), which makes it numerical intractable. On the one hand, the decision variables (the entries of the matrix $\boldsymbol{X}(\boldsymbol{\rho})$) can have an arbitrary functional dependence on the parameters of the considered system. On the other hand, the constraints depend on the system parameters, so that an infinite number of LMIs has to be considered. Remedies from the literature for both problems are presented below.

In order to avoid the functional dependence of the decision variable $\boldsymbol{X}(\boldsymbol{\rho})$, Wu [19] proposed to assign n_f basis functions

$$\boldsymbol{X}(\boldsymbol{\rho}) \coloneqq \sum_{i=1}^{n_\mathrm{f}} \mathrm{f}_i(\boldsymbol{\rho}) \boldsymbol{X}_i, \quad \text{where } \boldsymbol{X}_i \in \mathbb{S}^{n_x}. \tag{9}$$

The new decision variables are the coefficients $\boldsymbol{X}_i$ of the basis functions $\mathrm{f}_i(\boldsymbol{\rho})$. More basis functions obviously reduce the conservatism. However, since every basis function increases the number of the decision variables, this slows the optimization process down or may cause severe numerical problems. Consequently, the selection of the basis functions is an important step, which can have a crucial effect on the results. Unfortunately, there are hardly any guidelines in literature how to do this, but simple polynomials lead to good results in practice.

The simplest and maybe most popular way to avoid infinite dimensional LMIs is introduced in [19] and is based on a gridding of the parameter space. This means that the constraints are only enforced on a finite subset $\mathcal{P}_\mathrm{grid} \subset \mathcal{P}$. Because this is a mere approximation of the original problem, sufficiency is lost. It is thus self-explanatory that the density of the grid must be carefully chosen. In order to check the validity of the results, it is possible to optimize the performance index γ again with the obtained Lyapunov matrix on a second, much finer grid. A slight increase of the new performance index indicates – but does not prove – the validity of the results. However, the fact that sufficiency is lost should not be overrated. Even in the μ-framework, the analysis is often performed on a finite grid of frequency points. Moreover, an intensive benchmark study in [10] confirms the validity of the gridding approach.

4 Performance Analysis of LTI Models

The aim of this section is to show how the energy-to-peak gain can be used to compute upper bounds for loads resulting from "1-cosine" gust excitations. First, the aircraft model is presented. Next, a weighting filter is introduced. Afterwards, the energy-to-peak gain is compared to simulation results at a representative flight condition. Following this, it is shown how the trim loads can be included in the analysis. Finally, the comparison is generalized to the entire flight envelope.

4.1 Aircraft Model

As explained in the introduction, this paper aims to investigate how the robust performance analysis can be used for loads analysis. In order to yield meaningful conclusions, a model of industrial complexity for a generic transport aircraft is used. The comparison is pursued at the example of the wing root bending (WRB) moment P_WRB and the vertical acceleration $\ddot{u}_z$. The considered model input is the vertical wind v_gust, due to turbulence or gusts. Here, an open loop configuration is analyzed.

The model is based on the generalized linear equations of motion, which are typically used for gust and turbulence loads analysis. Due to the symmetric excitation in the considered scenario, it is sufficient to use only the heave and pitch rigid body mode. Moreover, 20 symmetric flexible modes are used. The loads are recovered using the force summation method. For details, see e. g. [9].

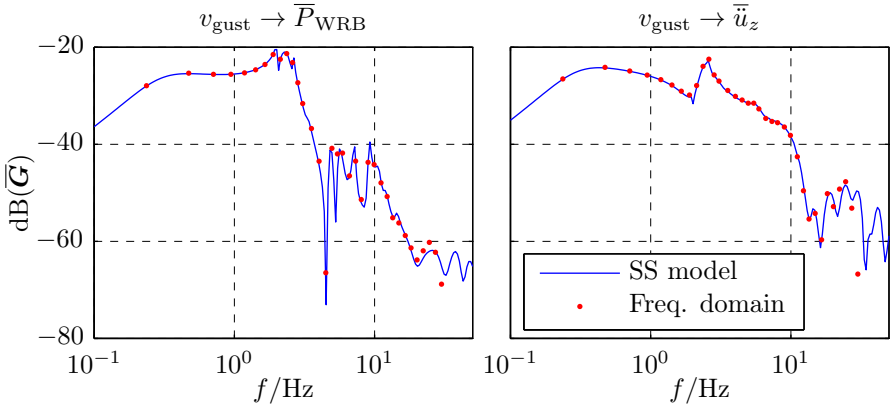

Figure 1: Comparison of the Bode diagrams of the state space aircraft model with the more common frequency domain model. A very good agreement can be observed.

The aerodynamics are modeled using the vortex lattice method and doublet lattice method. In order to obtain a state space representation, a rational function approximation (RFA) of the unsteady aerodynamic influence coefficient matrix is performed with a number of 8 poles, [9]: to capture the spiral nature of the gust column, the gust model is divided in 20 zones, each having its own reference point. The time delay between the collocation point and the preceding reference point is considered in the RFA. To include the delay between the reference points, Pad approximations of the dead time are applied. See [7] for details.

In order to cover the entire flight envelope, aerodynamic models are built for the Mach numbers $Ma \in \{0.50, 0.55, \ldots, 0.90\}$ and for the flight levels $h \in \{0.0\,\text{km}, 0.5\,\text{km}, \ldots, 10\,\text{km}\}$. However, some permutations are outside of the valid flight envelope and only the 133 valid combinations are considered below.

Connecting the aerodynamic models with the structure model yields 133 state space models with 236 states each. A Bode diagram of a normalized model[3] at a representative flight condition is depicted in Figure 1. Moreover, the Bode diagram of a model obtained by the more common frequency domain approach is shown and a very good agreement can be seen.

It is finally noted, that the total loads are composed by the $1g$ trim loads and by the dynamic response, e. g. for the WRB moment

$$P_{\text{WRB}}^{\text{total}} = P_{\text{WRB}}^{\text{trim}} \pm P_{\text{WRB}}. \tag{10}$$

The reason for the $\pm$ sign is that the wind can be directed upwards or downwards, which changes the sign of gust loads.

4.2 Weighting Filter

In order to yield significant results by a performance analysis, it is often necessary to add a weighting filter W, for example to weight the relevant frequency range, see Figure 2. In the considered case, the energy-to-peak gain is used to compute an upper bound for the loads due to "1-cosine" gust excitations. For that reason, a pre-filter must be able to shape a "1-cosine" gust of arbitrary length with an maximum energy of $\|d\|_{\mathcal{L}_2} \leq 1$. This can be achieved by a suitable choice of the parameters k and T of the first order low-pass filter

$$W := \left\{ \begin{array}{rl} \dot{x}_W = & -\frac{1}{T}\, x_w + \frac{k}{T}\, d \\ v_{\text{Gust}} = & x_w \end{array} \right. . \tag{11}$$

It has to be mentioned, that the weighting filter has to be adapted for every flight condition: the time constant T has to be adapted to the aircrafts true airspeed and the gain k according to the design gust velocity [1].

[3] Note that the normalization of any parameter $(\cdot)$ is indicated by overlining it $\overline{(\cdot)}$.

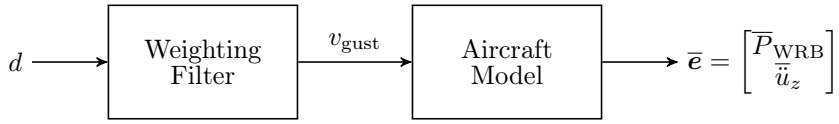

Figure 2: Aircraft model with weighting filter.

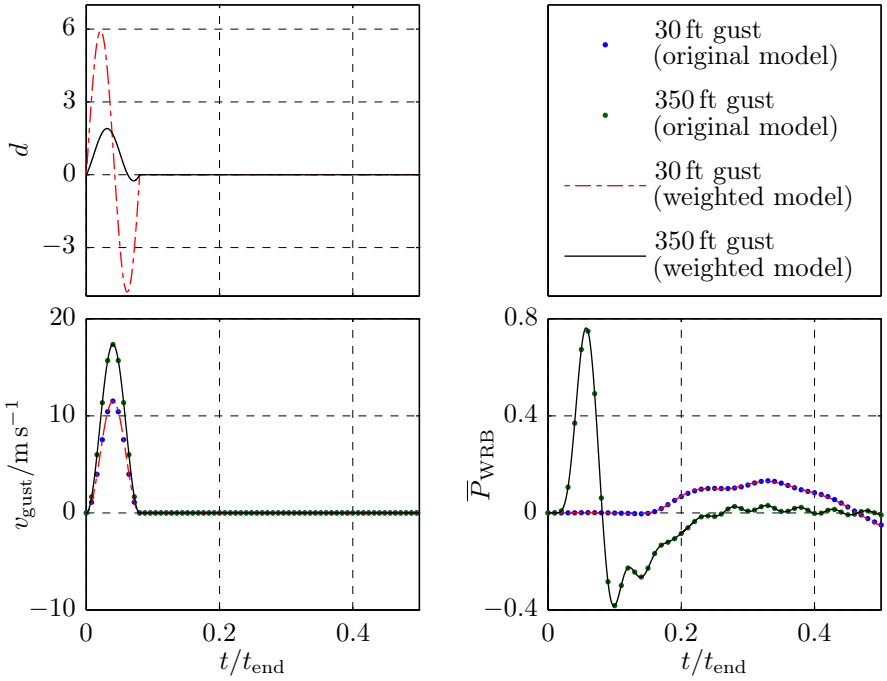

Figure 3: Validation of the weighting filter. The disturbances $d(t)$ are designed such that the corresponding filter output matches the considered "1-cosine" gust and that $\|d\|_{\mathcal{L}_2} \leq 1$. (Please note the different scalings of the time axis.)

Simulation results for the 30 ft and the 350 ft gust as defined in [1] are presented in Figure 3. Note that in order to clearly depict the results, the scaling of the time axis is adapted to the considered gust length. In the upper left subplot, the input to the weighting filter can be seen. The signals are designed such that the corresponding filter output matches the considered "1-cosine" gust and that $\|d\|_{\mathcal{L}_2} \leq 1$. In the lower left subplot, the output of the filter and the actual gust are depicted. A perfect agreement can be seen. Finally, in the right subplot, the output of the unweighted model (directly excited by the gust) and the output of the weighted model (excited by $d(t)$) are shown. Again, a perfect agreement can be seen. The same result is obtained for the vertical acceleration.

4.3 Analysis Results at one Flight Point

Simulations with the original model for seven different gust lengths between 30 ft and 350 ft are performed and the results are depicted in Figure 4. In addition, the energy-to-peak norm of the weighted model is computed (separately for both transfer paths) and also illustrated in Figure 4. Since the weighting filter can shape an arbitrary "1-cosine" gust, the simulation results do not exceed the norm. Moreover, it can be guaranteed that there exists no gust length in the range between 30 ft to 350 ft which exceeds the norm.

Another important result is that the worst of the considered seven gusts reaches 71 % and 72 % of the energy-to-peak norm. An over-estimation of loads by 40 % is certainly significant. However, the estimation is in the correct order of magnitude so that the information is still valuable.

It is further possible to compute the worst disturbance $d(t)$ with unit energy, which actually reaches the norm by the matched filter theory, see [20]. This result is depicted in Figure 5. In the left subplot the disturbance $d(t)$ is shown. In the middle, the weighting filter output – so the actual gust – can be seen. In the right subplot, the resulting WRB moment is depicted and it can be seen

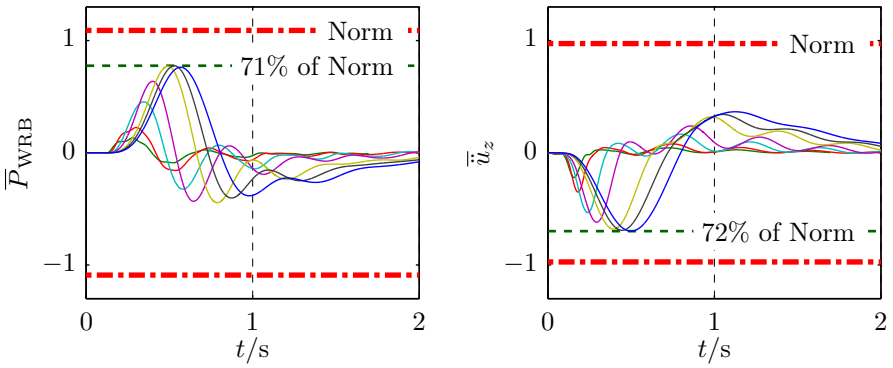

Figure 4: Comparison of the results from gust simulations with the worst case energy-to-peak gain.

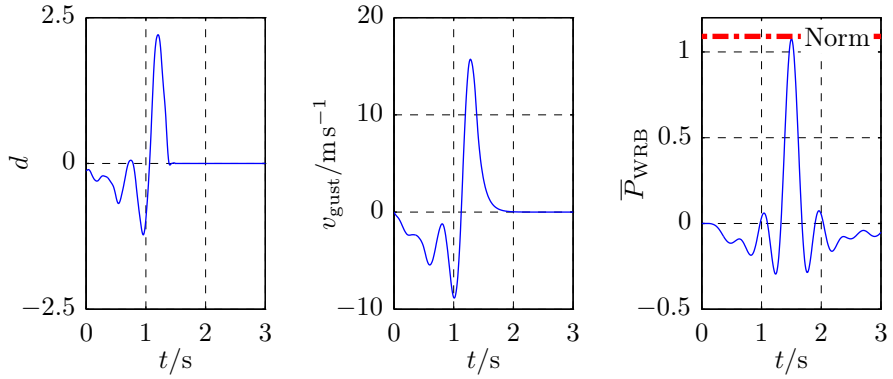

Figure 5: Worst case excitation for the WRB moment. The induced $\mathcal{L}_2$-$\mathcal{L}_\infty$ norm is reached.

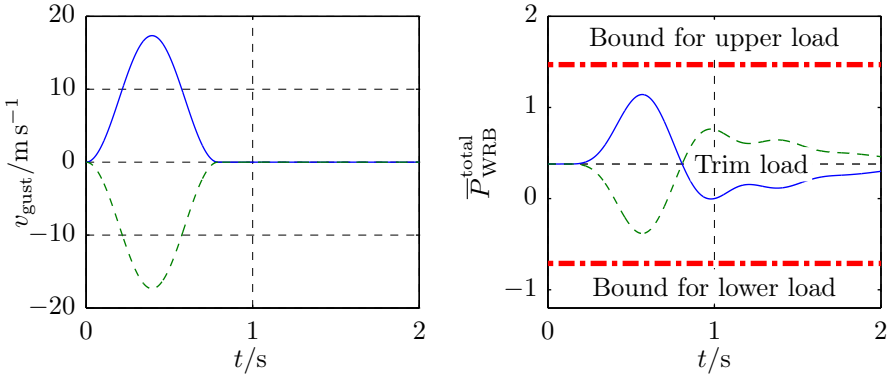

Figure 6: Bound for lower and upper load including the trim load at the example of the 350 ft gust.

that the norm is reached. Again, a similar result is obtained for the vertical acceleration.

4.4 Inclusion of Trim-Loads

As already mentioned, the trim loads have to be considered to yield the total loads. Similar to the normal loads computation process, this can be achieved by superimposing the norm with the trim loads. This leads to the following bounds for the maximum and minimum loads:

$$P^{\mathrm{trim}}_{\mathrm{WRB}} - \|G_{d,P_{\mathrm{WRB}}}\|_{\mathcal{L}_2\to\mathcal{L}_\infty} \leq P^{\mathrm{total}}_{\mathrm{WRB}} \leq P^{\mathrm{trim}}_{\mathrm{WRB}} + \|G_{d,P_{\mathrm{WRB}}}\|_{\mathcal{L}_2\to\mathcal{L}_\infty}\,. \tag{12}$$

This is illustrated in Figure 6. Loads resulting from an upwards and a downwards directed 350 ft gust are superimposed with trim loads. The total loads do not exceed the bounds from (12). Only the gust loads are considered below, since the norm covers only the gust increment.

4.5 Analysis Results for the Complete Flight Envelope

In order to validate the results, the analysis from the preceding section is repeated for the entire flight envelope and the results are depicted in Figure 7. In the left column the WRB moment is considered and in the right one the vertical acceleration. In the first row, the maximum peak of all simulations at one flight point is plotted as a function of the true air speed v_{TAS} and the flight level h. The maximum loads occur for high velocities and low flight levels. This agrees to the physical consideration that the maximum loads occur, where the dynamic pressure is maximal. In the second row, the induced $\mathcal{L}_2$-$\mathcal{L}_\infty$ norms are plotted in the same manner. Obviously, the trend of the peaks and of the norms have almost the same shape. The ratios of the maximum peaks and of the energy-to-peak gains are depicted in the last row. It can be seen that the ratios never exceed a value of one. This confirms again that the norm provides an upper bound for the loads. Further, the ratio varies only slightly between 62 % and 77 %. Consequently, the energy-to-peak norm is as an excellent indicator for critical flight conditions.

Finally, the computation times are compared. The required time to compute the energy-to-peak norm for all 133 flight conditions is 16 s. On the contrary, the computation time for the "1-cosine" gust simulations is 1.85 h. The computation via the norm is thus more than 400 times faster. Certainly, this result has to be put into perspective that a frequency domain computation of loads is faster than a simulation in the time domain.

Summarizing, it can be stated that the energy-to-peak gain can be used to quickly compute useful bounds for loads resulting from "1-cosine" gust excitations.

5 Robust Performance Analysis of a Parametric Model

Finally, the robust performance analysis is used to compute an upper bound for the energy-to-peak gain, which is not only valid for one flight condition but for a specific parameter range. In the considered scenario, the altitude h is assumed to be uncertain in the interval from 0 km to 10 km, while the Mach number is held constant at $Ma = 0.5$.

To this end, the weighted models at $Ma = 0.5$ from Section 4 are used and a grid based LPV model is derived. The considered model parameter is the flight level, which changes – at least for civil transport aircrafts – such slowly that a zero parameter bound is assumed. In order to obtain a reasonable problem size, the LPV order reduction from [15] is applied to create a grid based LPV model with 25 states. The original and the reduced model are compared in Figure 8 and an excellent agreement can be clearly seen. Moreover, the relative error measured by the induced $\mathcal{L}_2$-$\mathcal{L}_\infty$ norm is less than 2 % at all grid points.

The analysis results are compiled in Table 1. As a reference, the maximum LTI norm of all grid points is computed by solving the Lyapunov equation. The LPV analysis is performed by the gridding approach. The SDP is solved using only every second grid point, referred to as rough grid. This allows to validate the results on the full grid. First, a quadratic basis function for the Lyapunov matrix is used. Since the solution of the rough grid fulfills the LMIs also on the full grid, it is concluded that the solution is valid. However, since the result is approximatively twice as large as the maximum LTI norm, the result is considered to be too conservative. Consequently, a cubic basis function is used and the analysis is repeated in the same way. In that case, the robust induced $\mathcal{L}_2$-$\mathcal{L}_\infty$ norm is only slightly greater than the maximum LTI norm.

The advantage of this approach is that by only one analysis an upper bound for a complete parameter space can be computed without any danger of missing a critical flight condition. A large gap between the maximum LTI norm and the LPV norm can be indicative for conservatism. Another explanation for a large gap is that too few grid points for the LTI analysis have been used. Finally,

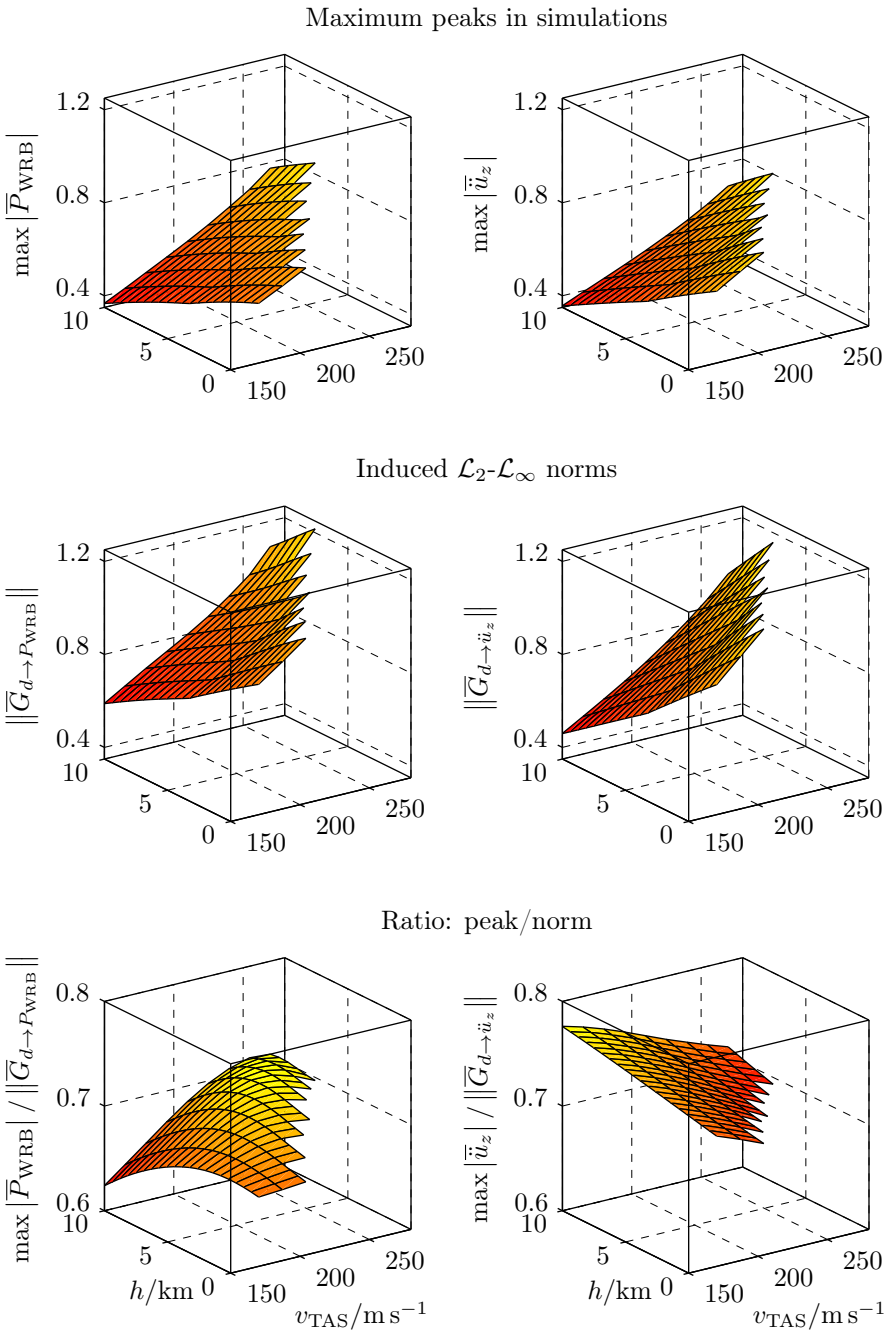

Figure 7: Peaks from gust simulations are compared with the worst case energy-to-peak gain for the complete flight envelope.

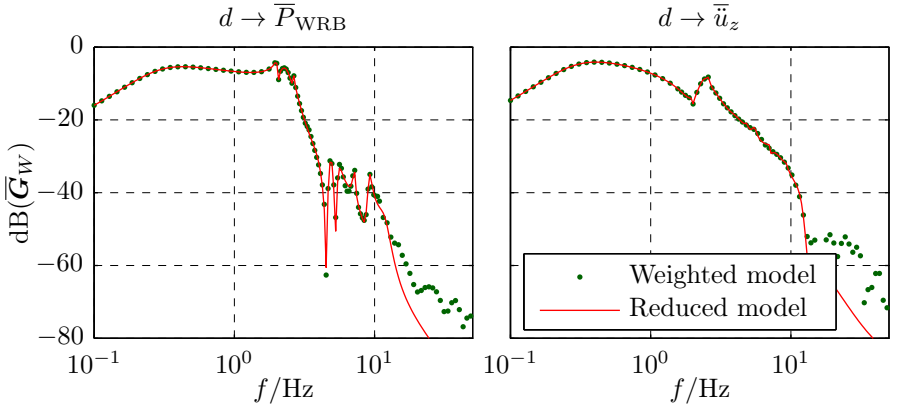

Figure 8: Bode diagram of the weighted and the reduced model at one flight point.

$\boldsymbol{X}(\rho)$	$\left\|\overline{\boldsymbol{G}}_{d\to P_{\mathrm{WRB}}}\right\|$		$\left\|\overline{\boldsymbol{G}}_{d\to \ddot{u}_z}\right\|$	
	Rough grid	Full grid	Rough grid	Full grid
max LTI	N/A	0.910	N/A	0.909
quadratic	1.497	1.498	2.152	2.152
cubic	0.955	0.959	0.924	1.065

Table 1: LPV analysis results.

these grid points whose LTI norms are closest to the LPV norm are supposedly the critical ones.

6 Summary and Outlook

The versatile possibilities of the robust performance analysis framework for loads computation are demonstrated. It is shown how the worst case energy-to-peak gain can be used to compute a close but guaranteed upper bound for loads due to "1-cosine" gust excitations. It is further shown that there exists an excitation which reaches the computed upper bound. Finally, it is demonstrated how a robust performance analysis can be used to identify the worst flight condition without any danger of missing a critical point.

This paper is only a first step in using the robust performance analysis framework for loads computation and there are still many open questions. First, it should be possible to reduce the gap between the peak of the "1-cosine" gust simulation and the LTI norm: Since the worst excitation is shaped by the weighting filter, improving the filter could reduce the conservatism. Another point are nonlinearities, e. g. the flight control system. They can be considered by integral quadratic constraints (IQCs), which allow to treat many nonlinearities like saturation and dead zones, [14]. Next, the LPV performance analysis can be performed with more uncertain/varying parameters: for example, it is possible to handle not only the flight level but simultaneously the Mach number. Moreover, time varying parameters can be considered. Finally, there is the question how much the ratio between the peaks from simulation to the norm depends on the considered output. To investigate this, a study with a full aircraft model with more than 1500 outputs is planned. However, in order to compute correlated loads, which are needed in the further design/certification process, time simulation responses of the identified critical points will still be required.

Despite of these many open issues, the robust performance analysis framework seems to be a very promising approach for many problems in loads computation. Especially during a design optimization process it might be a valuable tool, since guaranteed bounds for loads can be quickly obtained.

Acknowledgment

The author wishes to thank his colleagues Thiemo Kier and Gertjan Looye for their idea to use the robust performance analysis framework for loads computation and for their support in all questions on loads computation. Moreover, the author wants to thank his former colleagues Florian Saupe and Harald Pfifer for their help in the robust performance analysis framework.

References

[1] European Aviation Safety Agency. *Certification Specifications and Acceptable Means of Compliance for Large Aeroplanes CS-25*, 2013.

[2] Dan Borglund. The μ-k method for robust flutter solutions. *Journal of Aircraft*, 41(5): 1209 – 1216, 2004.

[3] Marco Dettori and Carsten Scherer. Robust stability and analysis for parameter and dependent and systems using full block S-procedure. In *Conference on Decision & Control*. IEEE, 1998.

[4] Krzysztof J. Fidkowski, Frode Engelsen, Karen E. Willcox, and Ilan M. Kroo. Stochastic gust analysis techniques for aircraft conceptual design. In *12th AIAA/ISSMO Multidisciplinary Analysis and Optimization Conference*, 2008.

[5] Laurent El Ghaoui and Silviu-Iulian Niculescu, editors. *Advances in Linear Matrix Inequality Methods in Control*. SIAM, 2000.

[6] Frederic M Hoblit. *Gust loads on aircraft: concepts and applications*. AIAA, 1988.

[7] Mouti Karpel, B. Moulin, and P.C. Chen. Dynamic response of aeroservoelastic systems to gust excitation. In *International Forum on Aeroelasticity and Structural Dynamics*, 2003.

[8] Hamed H. Khodaparast, Georgia Georgiou, Jonathan E. Cooper, Luca Riccobene, Sergio Ricci, Gareth A. Vio, and P. Denner. Efficient worst case 1-cosine gust loads prediction. *Journal of Aeroelasticity and Structural Dynamics*, 2(2): 33–54, 2012.

[9] Thiemo Kier. An integrated loads analysis model including unsteady aerodynamic effects for position and attitude dependent gust fields. In *International Forum on Aeroelasticity and Structural Dynamics*, 2011.

[10] Andreas Knoblach, Mehran Assanimoghaddam, Harald Pfifer, and Florian Saupe. Robust performance analysis: a review of techniques for dealing with infinite dimensional LMIs. In *International Conference on Control Applications*. IEEE, 2013.

[11] Rick Lind and Marty Brenner. *Robust aeroservoelastic stability analysis*. Springer Verlag, 1999.

[12] Johan Lfberg. YALMIP: A toolbox for modeling and optimization in MATLAB. In *Proceedings of the CACSD Conference*, 2004.

[13] MathWorks. *Matlab Control System Toolbox: User's Guide*, 2011.

[14] Alexandre Megretski and Anders Rantzer. System analysis via integral quadratic constraints. *IEEE Transactions on Automatic Control*, 42(6): 819 – 830, 1997.

[15] Charles Poussot-Vassal and Clement Roos. Generation of a reduced-order LPV/LFT model from a set of large-scale MIMO LTI flexible aircraft models. *Control Engineering Practice*, 20: 919 – 930, 2012.

[16] Mario A. Rotea. The generalized $\mathcal{H}_2$ control problem. *Automatica*, 29 (2): 373 – 385, 1993.

[17] Sigurd Skogestad and Ian Postlethwaite. *Multivariable Feedback Control: Analysis and Design*. John Wiley & Sons, 1996.

[18] Kim-Chuan Toh, Michael J. Todd, and Reha H. Ttnc. SDPT3 – a MATLAB software package for semidefinite programming. *Optimization Methods and Software*, 11: 545 – 581, 1999.

[19] Fen Wu, Xin H. Yang, Andy Packard, and Greg Becker. Induced $\mathcal{L}_2$-norm control for LPV systems with bounded parameter variation rates. *International Journal of Robust and Nonlinear Control*, 6: 983 – 998, 1996.

[20] Thomas A. Zeiler. Matched filter concept and maximum gust loads. *Journal of Aircraft*, 34(1): 101–108, 1997.